Structure and morphology of segmented polyurethanes: 3. Electron microscopy and small angle X-ray scattering studies of amorphous random segmented polyurethanes

C. H. Y. Chen-Tsai, E. L. Thomas and W. J. MacKnight
Polymer Science and Engineering Department, University of Massachusetts, Amherst, Massachusetts 01003, USA

and N. S. Schneider
Organic Materials Laboratory, AMXMR-OP, Army Materials and Mechanics Research Center, Watertown, Massachusetts 02172, USA
(Received 19 March 1985)

Transmission electron microscopy and small angle X-ray scattering techniques have been applied to investigate the bulk morphology of compression moulded samples of an amorphous segmented polyurethane system. Samples of different hard segment content, from 13% to 74% by weight, were synthesized by solution polymerization, so that the hard segment sequence length distribution of each sample approximated the most probable distribution. Microscopy results indicate that meandering cylinders of the soft segment phase are present in the 74% sample. An alternating plate-like structure is found in the 52% sample. However, for samples of hard segment content lower than 50%, results from electron microscopy were inconclusive. The Percus–Yevick hard sphere liquid theory taking into account the polydispersity of domain size was applied to calculate the scattering behaviour of these lower hard segment content samples and compared with the experimental data. Modelling results and mechanical behaviour of these samples lead to the conclusion that discrete hard segment domains of anisotropic shape are present in the soft segment matrix. This conclusion is also supported by the results from calculations of specific area of domains. A spectrum of morphologies varying with sample composition is thus obtained for this particular system of polyurethanes.

(Keywords: amorphous segmented polyurethane; morphology; microdomain)

INTRODUCTION

Linear segmented polyurethane elastomers, first introduced by Schollenberger[1,2], have generated a great deal of technological and scientific interest because of their unusual physical and mechanical properties and their processability. Considerable attention has been devoted toward an explanation of structure–property relationships in these materials. Cooper and Tobolsky[3] compared the mechanical behaviour of block copolymers to that of linear segmented polyurethanes, and suggested the presence of microdomains in the latter on this basis. However, the first direct evidence for the existence of microdomains, reported by Bonart[4] and Clough *et al.*[5], were the results from small angle X-ray scattering (SAXS) studies. Prominent scattering peaks in the small angle range were found for semicrystalline as well as amorphous samples. The Bragg spacings of these peaks for a large number of polyurethane systems[6–9] are in the range of a few hundred Ångstroms. They were assumed to correspond to the interlamellar distance in the semicrystalline samples. It is however by no means certain that all polyurethane systems are lamellar, or if lamellar, for all compositions of a given system.

Transmission electron microscopy (TEM) studies of polyurethanes have been carried out on both semicrystalline systems and amorphous systems[9–17]. A few of the studies[10,11,14] used solvent casting techniques to prepare thin films for observation. These results do not represent the general morphology of segmented polyurethanes in the bulk, since the morphology varies with casting conditions and with the type of solvent used. Koutsky *et al.*[17] prepared thin films by solvent etching thick samples down to workable thickness for TEM observations. Sample thickness variation is expected, and artifacts may thus be induced. The solvent casting method used by Lagasse[10], curing thin films on mercury surface, suffers from the same defects. More importantly, the domain structure these authors showed in a few micrographs is probably an artifact due to the influence of the microscope transfer function under defocus conditions[18].

In previously published papers by the authors[15,16,19], the influence of reactant incompatibility on morphology and hard segment length of the bulk-polymerized segmented polyurethanes was investigated. Incompatibility among reactants may be a general effect in polyurethane systems. In addition to this factor, the degree of mixing of the reactant streams can also be important, especially in the fast reacting reaction injection moulding (RIM) processes[20]. The products obtained from

0032-3861/86/050659-08$03.00

bulk polymerization methods may thus be a multicomponent mixture[16,21] of homopolymer of soft or hard segments, statistical copolymers with various distribution of hard segment lengths, as well as some allophanate crosslinked material. Because in practice it is very difficult to maintain ideal reaction conditions, Peebles' calculations[22,23] of hard segment sequence length distributions for statistical random segmented polyurethanes are usually not applicable to the products from bulk polymerization processes.

The goal of the present work is to employ principally TEM and SAXS to monitor the effect of composition on morphology in an amorphous truly random segmented polyurethane system. With the knowledge of domain shape obtained from TEM, SAXS data can be analysed more accurately. Samples were made by a single-solvent homogeneous solution polymerization. A 90/10 mixture of 2,4- and 2,6-toluene diisocyanate (TDI) and 1,4-butanediol (BDO) was employed to form the hard segments. Hydroxyl terminated polybutadiene (HTPBD) endcapped by TDI was the soft segment. This system was chosen for three reasons. First, hydrogen bonding is restricted to occur only among hard segments, and thus phase separation is improved compared with the polyether and polyester based segmented polyurethanes. Second, no crystallinity is found for all samples under normal conditions. Third, the unsaturated double bonds in the soft segments provide for heavy atom staining to enhance the specimen contrast in the electron microscope.

EXPERIMENTAL

Materials

The HTPBD (Japan Synthetic Rubber) had a functionality of 1.97, a vinyl content of 55%, and $M_n = 2200$. Water was eliminated by distilling the water–chloroform azeotrope from the HTPBD and chloroform solution. This process was carried out under nitrogen. Both TDI (ICI) and BDO (DuPont) were distilled under low pressure before use. Tetrahydrofuran (THF) (Fisher, HPLC grade) was distilled and used as solvent in the solution polymerization process. Dibutyltin dilaurate was used as the catalyst.

Synthesis

Exact stoichiometric amounts of HTPBD and TDI were made into a 10% (by weight) THF solution with 0.01% (by weight) catalyst. The solution was kept at 68°C in a three-necked, round-bottomed flask equipped with stirrer and condenser. After 1 h of the endcapping reaction, 90% of the stoichiometric amount of BDO was added at once. $1\frac{1}{2}$ h later, the rest (10% of BDO) was added dropwise into the reactor, and the reaction proceeded for another $3\frac{1}{2}$ h to ensure completion of the reaction. No precipitation was observed at the end of the reaction. The solution was then poured into distilled water. The precipitated product was separated, washed and finally dried in the oven at 60°C.

The compositions of the samples are given in *Table 1*. Further details of the synthesis procedures and characterization of the final product are published in a separate paper[24]. Molecular weights and their distributions for all the products have been measured by gel permeation chromatography (g.p.c.), and results indicated that all the samples have their $\bar{M}_n$'s above 17 000. Tensile test results indicated that all the polymers showed superior properties to the previous bulk polymerized samples of the same chemical compositions[25].

Films that were 2 mm thick were made by compression moulding at temperatures 30°C above the hard segment glass transition temperatures and then quenched by running cold water through the hot plates. All sample films are transparent to light, and show no crystallinity by wide angle X-ray scattering and d.s.c. Sample films were stored at room temperature without direct exposure to light for at least four weeks before any experiments were conducted. This was to ensure that the existing morphology had reached a steady state, since it has been mentioned in the literature that some segmented polyurethanes have time dependent properties even at room temperature[5,25,26].

Cryo-ultramicrotomy

The samples were microtomed into thin sections for electron microscopy observations. A Reichert–Jung Ultracut with cryo thin-sectioning attachment, FC4, and glass knives were used. All microtomy was done by keeping the knife temperature at −70°C and the sample block temperature at −80°C. Both dry knife and wet knife (with the knife trough filled with propyl alcohol for floating sections) techniques were used. Sections were approximately 400 Å thick as determined experimentally according to the results of optical density measurements[27]. Sections were viewed either unstained or stained. For staining, sections were exposed to osmium tetroxide vapour for 4 h prior to TEM examination.

Electron microscopy

A JEOL 100 CX transmission microscope was operated at 100 kV at magnifications of 2000× to 33 000× using Kodak S0163 plates. Microtomed thin sections were observed directly without any support film. Special precautions were taken to minimize electron beam damage of the samples and avoid radiation artifacts by focusing on one area and translating to an adjacent area for recording. Stained sections were observed in-focus, while contrast in unstained sections was enhanced by underfocus of the objective lens[18].

Small angle X-ray scattering

SAXS data were taken at the Oak Ridge National Laboratory (ORNL) using the 10-metre SAXS apparatus. Cu Kα radiation was used at 35 kV and 40 mA with pinhole collimation. The 2-metre (short geometry) detector-to-sample distance was used to collect data over the angular range from 0.08°–1.5°. For the invariant calculation, SAXS data were taken up to 3° by using a 1-metre geometry. The scattered X-ray intensity $I(Q,\mu)$ was recorded by a two-dimensional position sensitive detector at different scattering angles Q and azimuthal angles μ, where $Q = (4\pi/\lambda)\sin\theta$; 2θ is the scattering angle and λ is the wavelength. Raw data were corrected for background noise, dark current and sensitivity of the detector before any further treatment.

RESULTS AND DISCUSSION

Electron microscopy

Samples of three compositions, 29%, 52% and 74% of hard segment content by weight, were selected for

extensive electron microscopy investigations. The mechanical properties, as determined by stress–strain analysis[24], showed a wide range of behaviour, from an elastomeric material (29% sample) to a higher modulus thermoplastic at high hard segment content (74% sample).

Figure 1a shows the morphology of the 74% sample. This particular bright field micrograph was taken at in-focus conditions from an OsO_4 stained thin section. The dark phase is the polybutadiene soft segment phase. Though the electron microscopy can only reveal the two dimensional projection of the three dimensional object, by viewing different areas which represent different cross-sectional projections of the system, essential information can be obtained about the three dimensional morphology. In the rectangular area, both dark and light phases are parallel and the average width of each phase is 11 nm (while in the circled area, the dark phase appears as round regions with an average diameter also of 11 nm, surrounded by a light matrix. It is apparent that the butadiene segments form cylindrical domains with an average diameter of 11 nm. *Figure 1b* shows that the dark stained soft segment phases (arrowed) are elongated along the edges of cavities. In these deformed areas it is quite clear that the hard segment phase (the light phase) is continuous. This conclusion agrees with the results of our recent gas diffusion experiment on the same sample indicating that the low transport phase (the hard segment phase) is continuous[28]. Unstained specimens were also examined, and similar results were obtained by employing phase contrast imaging techniques.

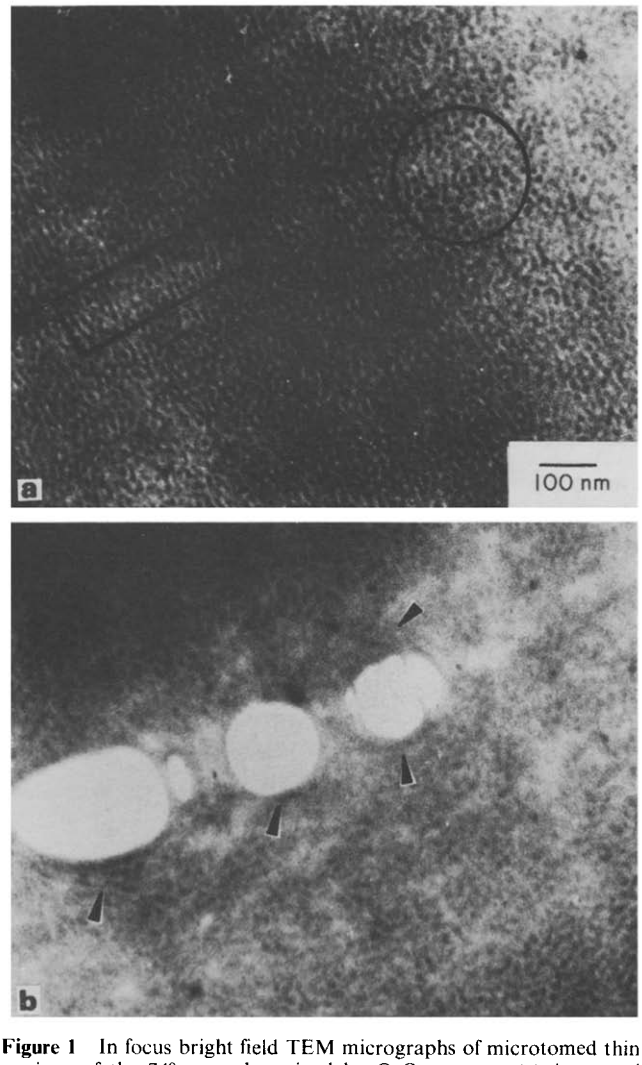

Figure 1 In focus bright field TEM micrographs of microtomed thin sections of the 74% sample stained by OsO_4 vapour. (a) A general morphology, and (b) a particular thin area due to the presence of cavities

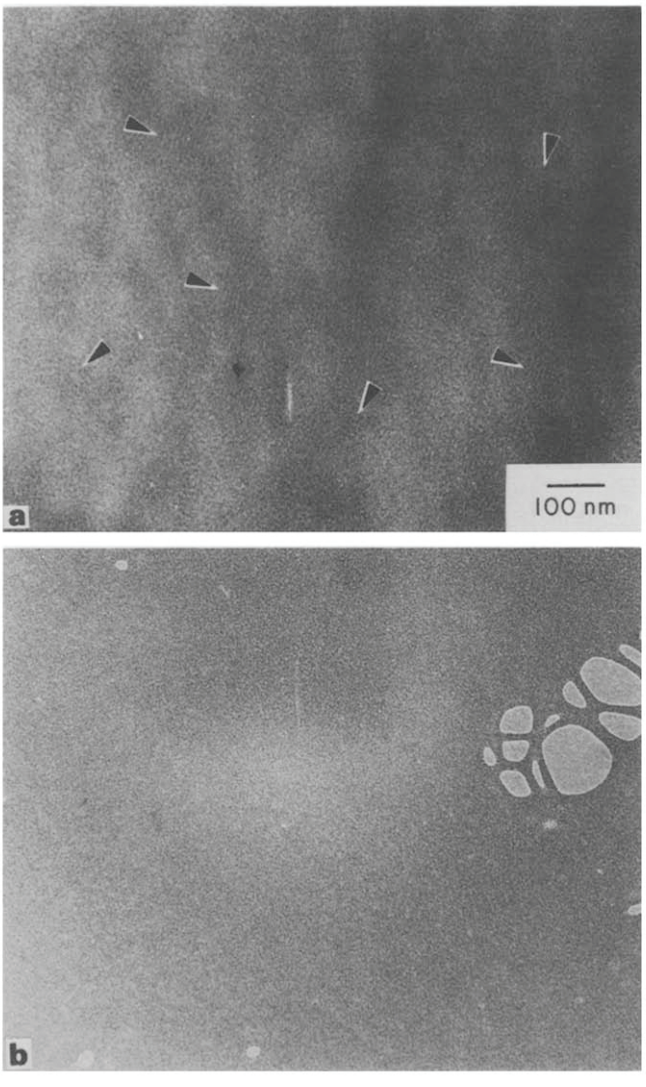

Figure 2 Underfocus bright field TEM micrographs of (a) an unstained microtomed thin section of the 52% sample, and (b) a homogeneous carbon thin film at same amount of defocusing

An underfocused (about 20 μm) micrograph (*Figure 2a*) taken from a thin unstained section of the 52% sample shows sets of parallel light and dark lines as indicated by arrows. This indicates that both soft and hard segment phases are plate-like. The average interdomain distance (defined as the centre to centre spacing of dark or white fringes) is 13 nm. This number agrees quite well with the SAXS results of the same sample which will be discussed later. It is clearly shown in *Figure 2a* that different sets of parallel lines (arrowed) are in different orientations, and this type of structure appears in every thin section of the 52% sample that has been examined. For comparison, an image of a homogeneous evaporated carbon film of similar thickness was obtained by operating the microscope at the same conditions as for the thin sections of the 52% sample (see *Figure 2b*). Notice the background of black and white speckles in the carbon film specimen. This effect originates from the influence of the microscope

transfer function on a white noise spectrum of the projected specimen potential (due to random density fluctuations in the sample) and was previously interpreted as a hard segment domain structure by Koutsky *et al.*[17]. OsO_4 stained specimens of the 52% sample were examined and a similar line structure was also found.

For lower hard segment content samples, no reliable information about the actual structure can be derived from the stained or unstained sections. This is because the two dimensional projection of the specimen inner potential is not interpretable when the size of the domain is much smaller than the thickness of the specimen; and at the same time either the domains are so densely but randomly distributed in the matrix (domain overlap problem), or the domains are so dilute and the inner potential difference between the two types of phases is so small, that the contrast is too low.

Small angle X-ray scattering

Scattering data over the angular range from 0.08°–1.5° were collected using the ORNL two dimensional detector using the short geometry for all the samples listed in *Table 1*. Isotropic intensity contours were obtained from all samples except the 74% and 52% samples. *Figure 3* shows the two-dimensional isointensity contour plot of the undeformed 52% sample. Some orientation is found in this sample as indicated by the slight anisotropy shown at very low angles. The 74% undeformed sample also demonstrated similar behaviour. The likely explanation for this is flow induced orientation during compression moulding. For systems containing microdomains of anisotropic shape (cylinders and lamellae in the above two cases), such a process may locally orient the domains. Although the 74% and 52% samples showed a very slight anisotropy at low angles, for the purpose of comparison, radial averaging was still applied to the data from these two samples.

In order to compare quantitatively the scattering power of each sample, all the scattering data were first corrected by background subtraction and sensitivity of the detector, and then normalized for sample thickness, transmission coefficient and counting time. *Figure 4* shows the plots of radially averaged intensities. Notice that every sample shows one rather prominent intensity maximum in the range which can be detected by the short geometry arrangement, and the maximum scattered intensity increases with hard segment content. The above two

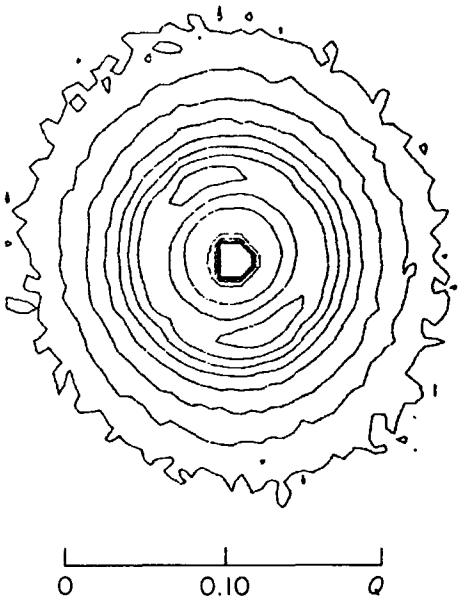

Figure 3 Isointensity contour plot of SAXS data for 52% sample. The first outside contour is 8 counts, and the succeeding ones are 65 counts plus the previous

Table 1 Compositions and molecular weights of the solution polymerized samples

Sample	HTPBD/TDI/BDO mole ratio	wt%[a] hard segment	vol%[b] hard segment	$\bar{M}_n$ from g.p.c. (ref. 24)
I	1/2.3/1.3	13	9	28 000
II	1/4.5/3.5	29	24	41 000
III	1/5.8/4.8	36	31	24 000
IV	1/6.8/5.8	40	35	60 000
V	1/8.7/7.7	47	42	35 000
VI	1/10.4/9.4	52	46	28 000
VII	1/25.2/24.2	74	69	17 000

[a] Hard segment content (% by weight)

$$= [(\text{moles of TDI} - 1) \times M_{TDI} + (\text{moles of BDO}) \times M_{BDO}] / [(\text{moles of HTPBD}) \times M_{HTPBD} + (\text{moles of TDI}) \times M_{TDI} + (\text{moles of BDO}) \times M_{BDO}] \times 100\%$$

where $M_{TDI} = 174$; $M_{BDO} = 90$; and $M_{HTPBD} = 2200$.

[b] Assuming no volume change during mixing and polymerization.

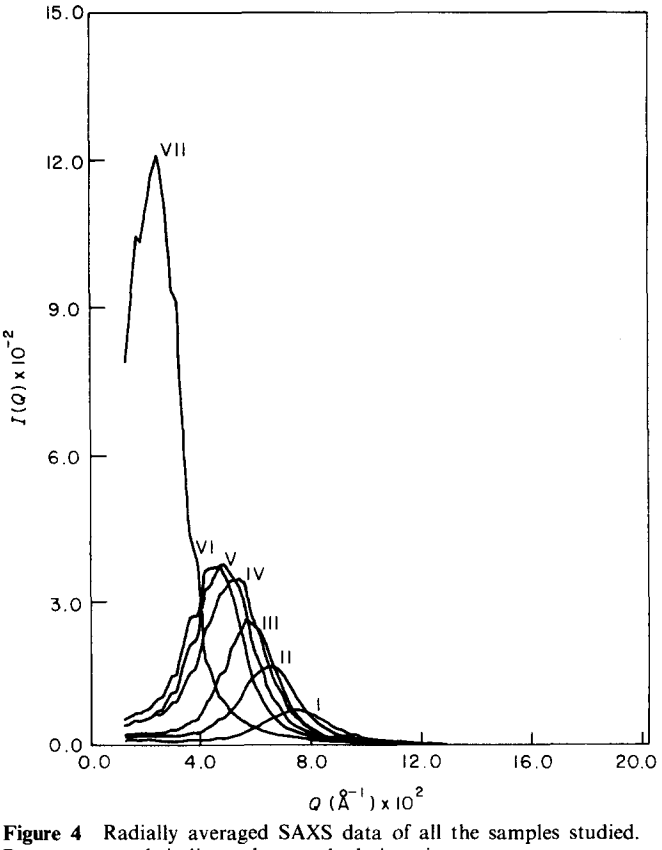

Figure 4 Radially averaged SAXS data of all the samples studied. Roman numerals indicate the sample designations

observations imply that microphase separation occurs in every sample. Both wide angle X-ray scattering (WAXS) and d.s.c. show no evidence of any crystallinity.

(i) *The high and medium hard segment content samples.* According to the electron microscopy observations, the 74% sample demonstrates a structure of meandering cylinders of the soft segment phase, and the average diameter of such cylinders is 11 nm. The radially averaged SAXS data of the same composition demonstrate a very sharp peak. If we (incorrectly) assume lamellae are present in the sample and multiply the scattered intensity by Q^2 (the Lorentz correction for a lamellar system), the corresponding Bragg spacing can be calculated. The result turns out to be 20 nm, a value that misrepresents the actual size of the microdomains as being obtained from TEM. The 52% sample, on the other hand, demonstrates an alternating plate-like structure from electron microscopy observations with an average width of a pair of dark and light plates being 13 nm. The radially averaged SAXS data of the same composition are corrected by Lorentz correction concerning the geometric symmetry of the lamellar structure (i.e. the scattered intensity is multiplied by Q^2). The average interlamellar distance is 13 nm. This value agrees very well with the result from electron microscopy. A discussion of the Lorentz factors for different morphological structures will be published separately[29].

(ii) *The low hard segment content samples.* In analogy to the morphology found in the amorphous di- or tri-block copolymers, it can be assumed that for samples of low hard segment content (< 30%) spherical hard segment domains are dispersed in the soft segment matrix. The polydisperse Percus–Yevick hard sphere liquid theory (PDPY) is applied to model the scattering curves of these low hard segment content samples. Kinning and Thomas[30] recently applied the PDPY theory to model the scattering curves of several block copolymers of spherical morphology. They also demonstrated the superiority of the PDPY theory over that of the Fournet hard sphere model[31].

Radially averaged SAXS data for samples of hard segment content from 13% to 36% by weight were modelled by the PDPY. In our curve fitting process, several parameters were used: (a) radius of spherical domains (R) which can be determined by the absolute value of the scattering vector where the maxima occurs in the form factor; (b) the effective hard sphere radius (R_{eff}) which includes R and the thickness of an impenetrable shell surrounding the spherical domain (see Figure 4 in ref. 30); (c) the standard deviation (σ_R) of the Gaussian type distribution of R and R_{eff} in the sample; (d) the effective hard sphere volume fraction (η) which is calculated from $[R_{\text{eff}}/R]^3\chi$, where χ is the volume fraction of the hard segment; and (e) the standard deviation (σ) of the Gaussian smearing function considering a diffuse domain boundary[32,33].

The procedure of curve fitting is to first calculate an initial value of R using Bragg's law (initial R equal to one half of the Bragg spacing), then vary R_{eff} (η will change accordingly) and σ_R to fit the scattering curve, and then take a better estimate of R and carry out the variations of R_{eff} and σ_R iteratively. Increasing the diffuse boundary thickness, σ, only decreases the scattered intensities at higher angles and is not very important in the present case. For practical purposes and also as a reasonable assumption for this polybutadiene based system, a sharp domain boundary, i.e. $\sigma = 0$, is considered for all samples.

The main difficulty encountered in the curve fitting process is illustrated in *Figure 5*. It has been mentioned that the SAXS curves of all the samples have a similar nature, i.e. giving one rather pronounced peak with a monotonic decrease of intensity at higher angles. When a good fit of the first interference peak (as indicated by arrow 2), predicted by the interference factor $S(Q)$, is obtained for a given set of parameters, there is always a shoulder in the calculated scattering intensity (as indicated by arrow 3) occurring right after the interference peak due to the first maximum from the sphere form factor $P(Q)$. If a broader sphere size distribution is used (i.e. increased σ_R), this shoulder will be smoothed while the intensities at lower angles (as indicated by arrow 1) will increase due to the nature of $S(Q)$ (see Figure 4 in ref. 34).

The values of parameters used in the 'good' fits for SAXS data of the three lowest hard segment content polyurethane samples are summarized in *Table 2*. Though

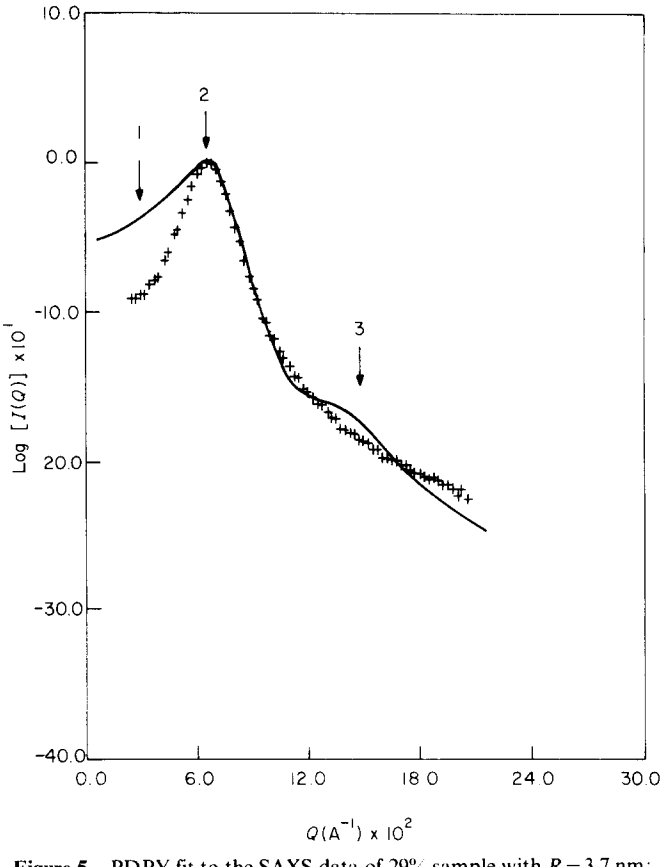

Figure 5 PDPY fit to the SAXS data of 29% sample with $R = 3.7$ nm; $R_{(\text{eff})} = 4.2$ nm; $\sigma_R = 0.6$ nm; $\eta = 0.36$ and $\sigma = 0.0$. Plot of log intensity *versus* Q

Table 2 Summary of parameters used in the polydisperse Percus–Yevick fit

Sample	$R_{(\text{eff})}$ (nm)	σ_R (nm)	R (nm)	η
I	4.1	0.3	2.5	0.37
II	4.2	0.7	3.7	0.36
III	5.0	0.8	4.5	0.42

$R_{(\text{eff})}$: effective hard sphere radius; σ_R: standard deviation of hard sphere size distribution; R: radius of spherical domain; η: effective volume fraction of hard spheres.

these values of R give a reasonable trend with increase of the hard segment content, the assumption of a spherical morphology in the low hard segment content polyurethanes cannot be satisfactorily justified by applying the present most general hard sphere theory. It appears problematical whether it is proper to draw an analogy of the morphology of the amorphous segmented polyurethanes to the amorphous block copolymers. Additional SAXS data from deformation experiments on these same samples, and the consideration of the sequence length distribution of the hard segment, however, strongly suggest the existence of microdomains with anisotropic geometry. Those results will be published in a separate paper[35].

Invariant calculations

SAXS two dimensional data for the 74%, 52% and 29% samples, over the scattering angle range from 0.08°–3.0°, were used in the invariant calculations. *Figure 4* shows that the scattered intensity peak of all the samples is well covered in this angular range, so there is no need to take lower angle (long geometry) measurements. A constant scattered intensity integrated over the volume of a sphere at very low angles was used to approximate the low angle contribution to the invariant of each sample.

It has been suggested in the past[36] that polydiene containing segmented polyurethanes have the sharpest interface among all commonly studied segmented polyurethane samples. The extreme incompatibility between the polybutadiene and the TDI/BDO hard segments has also been demonstrated by the authors[16,19]. It is quite reasonable then to describe the scattering behaviour of these HTPBD/TDI/BDO samples using the ideal two phase model. The ideal mean square electron density fluctuation, $\langle(\rho-\bar{\rho})^2\rangle_{\text{ideal}}$, can be calculated according to[37]

$$\langle(\rho-\bar{\rho})^2\rangle_{\text{ideal}}=\phi_1\phi_2(\rho_1-\rho_2)^2 \tag{1}$$

where ϕ_i and ρ_i are the volume fraction and mass density of phase i, respectively. The actual mean square electron density fluctuation, $\langle(\rho-\bar{\rho})^2\rangle_{\text{SAXS}}$, for an isotropic sample can be calculated according to[38]

$$\langle(\rho-\bar{\rho})^2\rangle_{\text{SAXS}}=4\pi/(N^2 i_e^2 PL\lambda^3)\int_{X=0}^{\infty}\int_{Y=0}^{\infty} XI(X,Y)\mathrm{d}X\mathrm{d}Y \tag{2}$$

where N stands for Avogadro's number, i_e is the Thomson scattering factor, t is the sample thickness, P is the power of the incident beam in counts/s (also known as the absolute intensity of the incident beam), L is the detector-to-sample distance, and X and Y (centimetres) are the coordinates of the two dimensional detector cells perpendicular to the incident beam direction. P was measured by using the nickel foil technique. Both $\langle(\rho-\rho)^2\rangle_{\text{ideal}}$ and $\langle(\rho-\rho)^2\rangle_{\text{SAXS}}$ have the units of (moles of electrons)^2/cm^6. Porod's law with consideration of thermal density fluctuation (Fl) is assumed to describe the scattering behaviour at high angles[39].

$$\lim_{Q\to\infty} I(Q)=K_p/Q^4+Fl \tag{3}$$

From a plot of $Q^4I(Q)$ vs. Q^4, K_p (the Porod-law constant) and Fl (a constant representing the scattering contribution from thermal density fluctuations) can be obtained. *Figure 6* shows the Porod plot for the 29% sample. It should be noticed that a positive deviation[32] from the ideal two phase model occurs. Such deviation can be explained in terms of thermal density fluctuations and the contribution of scattering from the wide angle regime.

Table 3 summarizes the results from the invariant calculations. The quantity $\langle(\rho-\rho)^2\rangle_{\text{SAXS}}/\langle(\rho-\rho)^2\rangle_{\text{ideal}}$ may be used to represent the degree of interfacial mixing*. The parameter D_{IM}, degree of interfacial mixing, can be defined as

$$D_{\text{IM}}\equiv 1-(\langle(\rho-\bar{\rho})^2\rangle_{\text{SAXS}}/\langle(\rho-\bar{\rho})^2\rangle_{\text{ideal}})^{1/2} \tag{4}$$

The values of D_{IM} (also given in *Table 3*) for these polybutadiene based samples are consistently smaller than the values of D_{IM} for some polyether and polyester based polyurethane samples. For example, values of D_{IM}

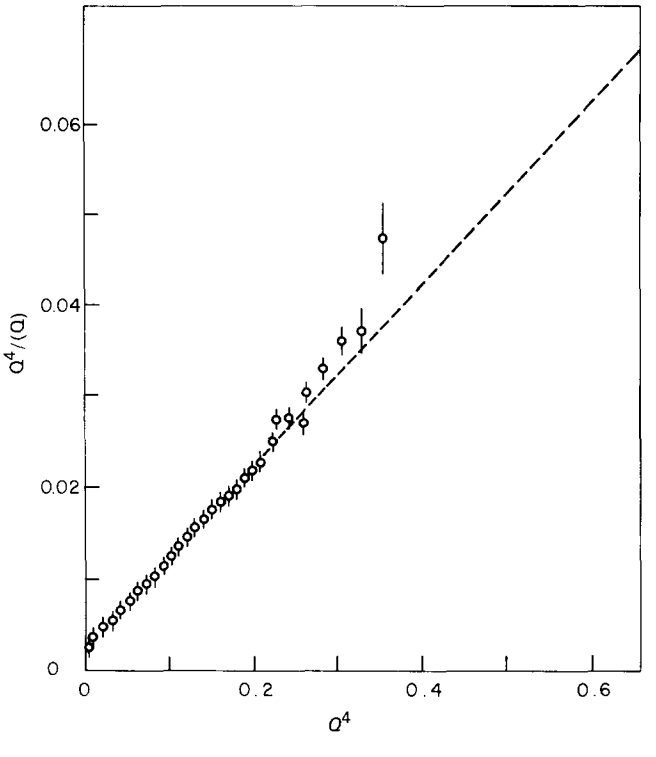

Figure 6 Porod plot of high angle SAXS data for the 29% sample

Table 3 Summary of the results from invariant calculations

Sample	ϕ_{HS}	Fl[a]	$\langle(\rho-\bar{\rho})^2\rangle_{\text{ideal}}$ $\left(\frac{\text{mole e}^-}{\text{cm}^3}\right)^2$	$\langle(\rho-\bar{\rho})^2\rangle_{\text{SAXS}}$ $\left(\frac{\text{mole e}^-}{\text{cm}^3}\right)^2$	D_{IM}
II	0.24	0.989	2.277×10^{-3}	2.153×10^{-3}	0.03
VI	0.46	1.186	3.019×10^{-3}	2.539×10^{-3}	0.08
VII	0.69	1.096	2.545×10^{-3}	2.464×10^{-3}	0.02

[a] The units for Fl are the same as for $I(Q)$, [(numbers of electrons)^2 × counts]/(cm^2 × s).

* Our definition is a modified version of that original given by Van Bogart *et al.*[40], where we normalize $\langle(\rho-\bar{\rho})^2\rangle_{\text{SAXS}}$ with respect to $\langle(\rho-\bar{\rho})^2\rangle_{\text{ideal}}$ of an ideal system with pure phases and sharp boundaries instead of normalizing with respect to a hypothetical system with partial phase mixing and sharp phase boundaries.

ranging from 0.15 to 0.35 were reported by Van Bogart *et al.*[40]. These results indicate that the polybutadiene samples have the sharpest domain interface among the three types of segmented polyurethanes.

The values of $\langle(\rho-\bar{\rho})^2\rangle_{SAXS}$ reveal that the 52% sample has the largest scattering power among the three samples. This is reasonable because the product of the volume fractions of hard and soft segment reaches its maximum value when the composition of the sample is 50/50. However, it is found that this value of $\langle(\rho-\rho)^2\rangle_{SAXS}$ for the 52% sample is about 15% smaller than the value calculated from the ideal two phase model. This relatively large deviation from the ideal value was also reported by Van Bogart *et al.*[40] for polycaprolactone based samples with ϕ_{HS} close to 50%. The reason for this drop in mean square electron density fluctuation is not very clear at this stage.

Notice that the above ideal mean square electron density fluctuation was calculated based on the assumption that all the hard segments (including hard segments with only one hard segment unit) phase separate from the soft segments and segregate into domains with sharp interfaces. If one assumes all the hard segments with only one hard segment unit are dissolved in the soft segment phase, and the hard segment sequence length distribution of each sample is of the most probable form[22,23], the resulting values of D_{IM} are still of the same order of magnitude. Because of the large difference in reactivity between the two isocyanate groups of TDI, the actual distribution of hard segment sequence length should be narrower than the most probable distribution. Also, in practice only a fraction of hard segments are dissolved in the soft segment phase if they do not totally phase separate. Nevertheless, the values of D_{IM} listed in *Table 3* still give a good indication of an overall low degree of interfacial mixing in this polybutadiene containing segmented polyurethane system.

From the value of K_p, it is possible to calculate the specific area, S/V, according to the following equation[41,42]

$$K_p=(S/V)U/(8\pi^3\phi_1\phi_2)=U/(2\pi^3 l_p) \tag{5}$$

where

$$U=4\pi\int_0^\infty Q^2 I(Q)\mathrm{d}Q \tag{6}$$

By rearranging equation (5), one has

$$(S/V)=8\pi^2\phi_{HS}(1-\phi_{HS})K_p/U \tag{7}$$

The Porod inhomogeneity length, l_p, can also be obtained by

$$l_p=U/(2\pi^3 K_p) \tag{8}$$

The inhomogeneity length of a given phase i can be calculated from l_p according to

$$l_i=l_p(1-\phi_i) \tag{9}$$

The physical meaning of l_i can be described by imagining a two phase system being pierced in all directions at random by rays[37]. The mean length of all the line segments intercepted by the hard segment phase is l_{HS}, and by the soft segment phase l_{SS}. *Table 4* summarizes the results from the above calculations along with the values of K_p. It is interesting to note that the value of l_{SS} is rather close to the value of cylindrical diameter determined by TEM for the 74% sample. This can be due to two possible reasons. If the cylindrical microdomains are randomly distributed in space, then either the aspect ratio of these domains should be very close to 1, i.e. short cylinders, or the cylinders can be long but meandering. The latter was what we observed by TEM from the same sample. The values of l_{HS} and l_{SS} for the 52% sample are found quite close to each other. This also agrees with the TEM observation that the thickness of both the hard and soft segment lamellar phases are rather similar.

Table 4 Summary of the results calculated from K_p's

Sample	K_p[a]	S/V (cm^2/cm^3)	l_{HS} (nm)	l_{SS} (nm)
II	2.550×10^{-4}	2.424×10^6	3.9	12.5
VI	1.688×10^{-4}	2.397×10^6	7.5	8.6
VII	7.844×10^{-5}	1.065×10^6	26.0	11.6

[a] The unit for K_p is the same as for $Q^4I(Q)$

The value of S/V indicates that a spherical domain morphology is not suitable to describe the morphology of the 29% sample. If spherical hard segment domains do exist, e.g. with a uniform radius of 3.7 nm, the S/V ratio calculated from such an assumption is 8×10^6 cm^{-1}. This value is more than two times larger than the S/V value given in *Table 4* for the 29% sample. If we allow a distribution of sphere sizes, restricted by the distribution of the hard segment length, more small spheres will be present than the large ones, and this will lead to an even larger S/V value than the value calculated from assuming uniform sphere size. The result of this comparison serves as an additional indication of the presence of hard segment domains with anisotropic shape in the low hard segment content samples.

CONCLUSIONS

Short meandering cylindrical domains of soft segments have been clearly imaged by transmission electron microscopy in a 74% compression moulded sample, and parallel plates of both hard and soft domains have also been imaged using the same technique for a 52% sample. However, for low hard segment content samples, results from electron microscopy are not conclusive due to the small size and the overlap of the microdomains. The results from small angle X-ray scattering studies indicate that these polybutadiene-based segmented polyurethane samples all had very sharp interfaces between the hard and soft segment phases. The parameter 'D_{IM}', which was redefined in this paper, was shown to be a useful relative measure of the degree of interfacial mixing. The inhomogeneity lengths of both hard and soft phases in the 76% and 52% sample calculated from their Porod constants were in good agreement with the size and shape of the microdomains observed by TEM. The SAXS data from the low hard segment content samples were modelled by the polydisperse Percus–Yevick hard sphere liquid theory assuming the presence of spherical hard segment domains with liquid-like order. The lack of fit suggests that the hard segment domains at low hard

segment content may have an anisotropic morphology. The values of specific area calculated from SAXS data also give the same indication. Thus, a spectrum of morphology of this model segmented polyurethane system is obtained.

ACKNOWLEDGEMENTS

The authors wish to acknowledge the Army Research Office, Durham, under grant No. DAAG 2980-C-0054. The authors are also pleased to acknowledge Dr J.-S. Lin at Oak Ridge National Laboratory and Mr D. J. Kinning at the University of Massachusetts for their technical assistance and helpful discussions.

REFERENCES

1 Schollenberger, C. S., Scott, H. and Moore, G. R. *Rubber World* 1958, **137**, 549
2 Schollenberger, C. S. US Pat. 2 871 218 (1/27/59)
3 Cooper, S. L. and Tobolsky, A. V. *J. Appl. Polym. Sci.* 1966, **10**, 1837
4 Bonart, R. *J. Macromol. Sci.–Phys.* 1968, **B2**(1), 115
5 Clough, S. B., Schneider, N. S. and King, A. O. *J. Macromol. Sci.–Phys.* 1968, **B2**(4), 641
6 Bonart, R., Morbitzer, L. and Hentze, G. *J. Macromol. Sci.–Phys.* 1969, **B3**(2), 337
7 Wilkes, C. E. and Yusek, C. S. *J. Macromol. Sci.–Phys.* 1973, **B7**(1), 157
8 Samuels, S. L. and Wilkes, G. L. *J. Polym. Sci. Symp.* 1973, **43**, 149
9 Schneider, N. S., Desper, C. R., Illinger, J. L., King, A. O. and Barr, D. *J. Macromol. Sci.–Phys.* 1975, **B11**(4), 5
10 Lagasse, R. R. *J. Appl. Polym. Sci.* 1977, **21**, 2489
11 Wilkes, G. L., Samuels, S. L. and Crystal, R. *J. Macromol. Sci.–Phys.* 1974, **B10**, 203
12 Aggarwal, S. L. *Polymer* 1976, **17**, 938
13 Fridman, I. D., Thomas, E. L., Lee, L. J. and Macosko, C. W. *Polymer* 1980, **21**, 393
14 Chang, A. L. and Thomas, E. L. in 'Multiphase Polymers' (Eds. S. L. Cooper and G. M. Estes), American Chemical Society, 1979, p. 176
15 Chang, A. L., Briber, R. M., Thomas, E. L., Zdrahala, R. J. and Critchfield, F. E. *Polymer* 1982, **23**, 1060
16 Chen, C. H. Y., Briber, R. M., Thomas, E. L., Xu, M. and MacKnight, W. J. *Polymer* 1983, **24**, 1333
17 Koutsky, J. A., Hein, N. V. and Cooper, S. L. *Polym. Lett.* 1970, **8**, 353
18 Roche, E. J. and Thomas, E. L. *Polymer* 1981, **22**, 333
19 Xu, M., MacKnight, W. J., Chen, C. H. Y. and Thomas, E. L. *Polymer* 1983, **24**, 1327
20 Kolodziej, P., Macosko, C. W. and Ranz, W. E. *Polym. Eng. Sci.* 1982, **22**(6), 388
21 Foks, J. and Janik, H. 'Proceedings of European Plastics Conference', Paris, June 1982
22 Peebles, L. H., Jr. *Macromolecules* 1974, **7**(6), 872
23 Peebles, L. H., Jr. *Macromolecules* 1976, **9**(1), 58
24 Bengston, B., Feger, C., MacKnight, W. J. and Schneider, N. S., in press
25 Brunette, C. M., Hsu, S. L., Rossman, M., MacKnight, W. J. and Schneider, N. S. *Polym. Eng. Sci.* 1981, **21**, 668
26 Schneider, N. S. and Matton, R. W. *Polym. Eng. Sci.* 1979, **19**, 1122
27 Flood, R. *Proc. SEM* 1980, **1**, 183
28 Serrano, M., Ottino, J. M. and Thomas, E. L., in preparation
29 Shibayama, M. and Thomas, E. L., in preparation
30 Kinning, D. J. and Thomas, E. L. *Macromolecules* 1984, **17**, 1712
31 Fournet, P. G. *Acta Cryst.* 1951, **4**, 293
32 Koberstein, J. T., Morra, B. and Steain, R. S. *J. Appl. Cryst.* 1980, **13**, 34
33 Hashimoto, T., Fujimura, M. and Kawai, H. *Macromolecules* 1980, **13**, 1660
34 van Beurten, P. and Vrij, A. *J. Chem. Phys.* 1981, **74**(5), 2744
35 Chen-Tsai, C. H. Y., Thomas, E. L. and MacKnight, W. J., in preparation
36 Desper, C. R., private communication
37 Alexander, L. E. in 'X-Ray Diffraction Methods in Polymer Science', R. E. Krieger Publ. Co., New York, 1979, pp. 290–291
38 Adams, W. W. *Ph.D. Dissertation*, University of Massachusetts, 1984
39 Ruland, W. *J. Appl. Cryst.* 1971, **4**, 70
40 Van Bogart, J. N. C., Gibson, P. E. and Cooper, S. L. *J. Polym. Sci., Polym. Phys. Edn.* 1983, **21**, 65
41 Kahovec, O., Porod, G. and Ruck, H. *Kolloid Z.* 1953, **133**, 16
42 Kratky, O. *Pure Appl. Chem.* 1966, **12**, 483